Time-dependent density functional theory (TD-DFT) coupled with reference interaction site model self-consistent field explicitly including spatial electron density distribution (RISM-SCF-SEDD)

D. Yokogawa

Citation: The Journal of Chemical Physics **145**, 094101 (2016); doi: 10.1063/1.4962062
View online: http://dx.doi.org/10.1063/1.4962062
View Table of Contents: http://scitation.aip.org/content/aip/journal/jcp/145/9?ver=pdfcov
Published by the AIP Publishing

Time-dependent density functional theory (TD-DFT) coupled with reference interaction site model self-consistent field explicitly including spatial electron density distribution (RISM-SCF-SEDD)

D. Yokogawa[1,2,a)]
[1]*Department of Chemistry, Graduate School of Science, Nagoya University, Chikusa, Nagoya 464-8602, Japan*
[2]*Institute of Transformative Bio-Molecules (WPI-ITbM), Nagoya University, Chikusa, Nagoya 464-8602, Japan*

(Received 7 May 2016; accepted 21 August 2016; published online 1 September 2016)

Theoretical approach to design bright bio-imaging molecules is one of the most progressing ones. However, because of the system size and computational accuracy, the number of theoretical studies is limited to our knowledge. To overcome the difficulties, we developed a new method based on reference interaction site model self-consistent field explicitly including spatial electron density distribution and time-dependent density functional theory. We applied it to the calculation of indole and 5-cyanoindole at ground and excited states in gas and solution phases. The changes in the optimized geometries were clearly explained with resonance structures and the Stokes shift was correctly reproduced. *Published by AIP Publishing.* [http://dx.doi.org/10.1063/1.4962062]

I. INTRODUCTION

Bioimaging technique is one of the most powerful approaches to study biosystems. To understand the functional in biosystems, many kinds of spectroscopic techniques have been proposed, such as two-photon absorption technique, stimulated emission depletion (STED) microscopy, single-molecule fluorescence imaging, and so on.[1,2] To accelerate the development of the techniques, a rational design of imaging molecules will play a key role.

The key point in the design is to understand the excited state of the imaging molecules in solution. The energy difference between ground and excited states is important information in color tuning and energy surface at excited state greatly affects the life time of the emission. How to obtain the information about the excited state in solution? The theoretical approach should be useful to study this excited state at atomistic and electronic structure levels.

There have been a variety of theoretical methods for excited state calculation in gas phase, such as time-dependent density functional theory (TD-DFT), configuration-interaction theory, multi-configurational self-consistent theory, coupled-cluster theory for excited state, and so on.[3,4] However, the number of methods that can treat an excited state in solution is limited to our knowledge. The difficult point is the computational cost of excited state calculation and the treatment of a large number of solvent molecules.

The most popular approach is TD-DFT coupled with polarizable continuum model (PCM).[5,6] TD-DFT gives the result at excited state with reasonable computational cost and PCM can replace the solvent molecules with a simple dielectric continuum model. This approach was implemented in many quantum chemical packages and has been applied to many kinds of systems.

Another approach is based on Reference Interaction Site Model (RISM) and RISM self-consistent field (RISM-SCF).[7–9] In RISM, the solvent molecules are replaced by the distribution of solvent atomic sites, and solute-solvent interaction is computed with the distributions. The interesting point in RISM is that these distributions can be obtained analytically by solving integral equations. Minezawa *et al.* coupled TD-DFT with RISM-SCF.[10,11] Because RISM gives solvation structure, TD-DFT coupled with RISM will be another important approach.

Although RISM approaches have such strong advantages, there were some disadvantages. The most severe problem was that solvation effect is enhanced in the original RISM.[12–14] This overestimation is much enhanced when we applied a diffuse basis set in the calculation.[14] This defect will be critical in excited state calculations because it is well known that excited-state electron densities can be much more diffuse than their ground-state analogues.[15] If we want to get reliable results for an excited state in solution with RISM, we have to solve this defect.

In this work, we derived equations for free energy and gradient calculations at excited state in solution on the basis of RISM-SCF explicitly including spatial electron density distribution (RISM-SCF-SEDD). As described in previous studies, our new density fitting approach overcame the defect in the original RISM-SCF.[12,14] To derive the equations of free energy and gradient at excited state in solution, we applied Lagrangian approach, which has been applied to the derivation of gradients.[16,17]

The organization of this paper is as follows. In Section II, we derive the equations for a method based on Lagrangian approach. Computational details are summarized in Section III. In Section IV, we compare our results with the previous data obtained by Minezawa by using a simple system, acetone in aqueous phase. We also check the reliability of our method by calculating indole and 5-cyanoindole in gas phase, in acetonitrile (AN), in methanol (MeOH), and in aqueous phase.

a)Electronic mail: d.yokogawa@chem.nagoya-u.ac.jp

II. METHODS

Before we derive equations for TD-DFT calculations in solution, we summarize RISM-SCF-SEDD[12,14,18] briefly. In RISM-SCF-SEDD, electron density at ground (G) or excited (E) state on the atomic site I is approximated with the sum of auxiliary basis set (ABS) $\{f_\alpha\}$,

$$\rho_I^{[\kappa]}(\mathbf{r}) = \sum_{\alpha\in I} d_{[\kappa]\alpha} f_\alpha(\mathbf{r}), \tag{1}$$

where κ means the calculated state, G or E. $\mathbf{d}_{[\kappa]}$ is the coefficient to be fitted and it is determined by the following equation:

$$\mathbf{d}_{[\kappa]} = \sum_{pq\sigma} (\Xi + \mathbf{\Gamma}^{[\kappa]})^{-1} \left\langle p\sigma \left| \hat{\mathbf{R}}' \right| q\sigma \right\rangle P^{[\kappa]}_{pq\sigma}. \tag{2}$$

$\mathbf{P}^{[\kappa]}$ is total electron density matrix at κ state with MO basis, where subscripts (p and q) are for the MOs and σ is for spin state. The elements of Ξ, $\mathbf{R}'$, and $\mathbf{\Gamma}^{[\kappa]}$ are defined by

$$\Xi_{\alpha\beta} = \begin{cases} \iint f_\alpha(\mathbf{r})|\mathbf{r}-\mathbf{r}'|f_\beta(\mathbf{r}')d\mathbf{r}d\mathbf{r}' & (\alpha,\beta \le M_{\mathrm{A}}), \\ 0 & (\alpha=\beta=M_{\mathrm{A}}+1), \\ -1 & (\text{otherwise}), \end{cases} \tag{3}$$

$$\hat{R}'_\alpha(\mathbf{r}) = \begin{cases} \int f_\alpha(\mathbf{r}_2)|\mathbf{r}-\mathbf{r}_2|d\mathbf{r}_2 & (\alpha \le M_{\mathrm{A}}), \\ -1 & (\alpha = M_{\mathrm{A}}+1), \end{cases} \tag{4}$$

$$\Gamma^{[\kappa]}_{\alpha\beta} = \begin{cases} -\mu \int \Theta^{(m-2)}[-\rho_I^{[\kappa]}(\mathbf{r})] f_\alpha(\mathbf{r}) f_\beta(\mathbf{r}) d\mathbf{r} & (\alpha,\beta \in I), \\ 0 & (\text{otherwise}), \end{cases} \tag{5}$$

where M_{A} is the number of ABSs. m and μ are parameters to make $\rho_I^{[\kappa]}(\mathbf{r})$ positive all over the space. $\Theta^{(l)}[x]$ is the truncated power function and is defined by

$$\Theta^{(l)}[x] = \begin{cases} |x|^l & (x>0), \\ 0 & (x\le 0). \end{cases} \tag{6}$$

When μ is 0, Eq. (1) becomes the same with the electron density derived in a previous study.[12] $\mathbf{\Gamma}$ is the penalty function that deters the fitted density from being negative. Although there are no unique parameters about m and μ, we found that large μ caused the fitted density to be positive over almost all space, as shown in Ref. 14. In this study, we employed the parameters $m = 6$ and $\mu = 10^{17}$.

A. Lagrangian for excited state calculation

We define the free energy at excited state in solution $\Delta G_{[\mathrm{E}]}$ by[19]

$$\Delta G_{[\mathrm{E}]} = \frac{1}{2}\sum_{i\sigma}(h_{ii\sigma} + F^{\mathrm{gas}}_{ii\sigma}) + \langle X,Y|\Lambda^{\mathrm{gas}}|X,Y\rangle + \Delta\mu_{[\mathrm{E}]} - \mathbf{V}^t_{[\mathrm{E}]}\mathbf{d}_{[\mathrm{Z}]}. \tag{7}$$

$\mathbf{F}^{\mathrm{gas}}$ is the Fock matrix defined in gas phase, $\mathbf{h}$ is the one electron integral in molecular orbitals, and $\Delta\mu_{[\mathrm{E}]}$ is solvation free energy at excited state. $V_{[\mathrm{E}]i}$ is the electrostatic potential on the ith ABS induced by solvent molecules and the solvation coordinate is computed at excited state. $\mathbf{d}_{[\mathrm{Z}]}$ is defined by

$$\mathbf{d}_{[\mathrm{Z}]} = \sum_{ia\sigma}\left[\Xi + (m-1)\mathbf{\Gamma}^{[\mathrm{E}]}\right]^{-1}\left\langle i\sigma\left|\hat{\mathbf{R}}'\right|a\sigma\right\rangle Z_{ia\sigma}. \tag{8}$$

$\mathbf{X}$ and $\mathbf{Y}$ are excitation vectors defined on the Hilbert space $L = L_{\mathrm{virt}}\times L_{\mathrm{occ}} \oplus L_{\mathrm{virt}}\times L_{\mathrm{occ}}$, where L_{occ} and L_{virt} denote the Hilbert spaces of occupied and virtual molecular orbitals (MOs), respectively.[17] As usual, we employ $i,j,\ldots$ label for occupied, $a,b,\ldots$ for virtual, and $p,q,\ldots$ for general MOs. Λ^{gas} is the matrix given by

$$\Lambda^{\mathrm{gas}} = \begin{pmatrix} \mathbf{A}^{\mathrm{gas}} & \mathbf{B}^{\mathrm{gas}} \\ \mathbf{B}^{\mathrm{gas}} & \mathbf{A}^{\mathrm{gas}} \end{pmatrix}, \tag{9}$$

and the elements are

$$A^{\mathrm{gas}}_{kc\sigma jb\sigma'} = (F^{\mathrm{gas}}_{cb\sigma}\delta_{kj} - F^{\mathrm{gas}}_{kj\sigma}\delta_{cb})\delta_{\sigma\sigma'} + (kc\sigma|jb\sigma') + f^{\mathrm{xc}}_{kc\sigma jb\sigma'}, \tag{10}$$

$$B^{\mathrm{gas}}_{kc\sigma jb\sigma'} = (kc\sigma|jb\sigma') + f^{\mathrm{xc}}_{kc\sigma jb\sigma'} - c_x\delta_{\sigma\sigma'}[(jc\sigma|kb\sigma) + (cb\sigma|kj\sigma)]. \tag{11}$$

$(pq\sigma|rs\sigma')$ is a two-electron repulsion integral and $f^{\mathrm{xc}}_{pq\sigma rs\sigma'}$ represents a matrix element of the exchange-correlation kernel. c_x is the hybrid mixing parameter introduced by Becke.[17,20]

To derive the equations required for the excited state calculation in solution, we define the following Lagrangian function:

$$\mathcal{L} = \Delta G_{[\mathrm{E}]} - \Omega(\langle X,Y|\Delta|X,Y\rangle - 1) + \sum_{ia\sigma} Z_{ia\sigma}F^{\mathrm{sol}}_{ia\sigma} - \sum_{pq\sigma,p\le q} W_{pq\sigma}(S_{pq\sigma} - \delta_{pq}). \tag{12}$$

By minimizing $\mathcal{L}$ with respect to $\mathbf{Z}$ and $\mathbf{W}$, we get the following equations:

$$F^{\mathrm{sol}}_{ia\sigma} = 0, \tag{13}$$

$$S_{pq\sigma} - \delta_{pq} = 0, \tag{14}$$

where $\mathbf{F}^{\mathrm{sol}}$ is the solvated Fock matrix, which was defined in previous works.[12,14] The Lagrangian multiplier Ω is determined by minimizing $\mathcal{L}$ with respect to X and Y, and the equation to be solved is

$$\Lambda^{\mathrm{sol}}|X,Y\rangle = \Omega\Delta|X,Y\rangle\,. \tag{15}$$

The elements of Λ^{sol} are

$$A^{\mathrm{sol}}_{kc\sigma jb\sigma'} = (\epsilon^{\mathrm{sol}}_{c\sigma} - \epsilon^{\mathrm{sol}}_{k\sigma})\delta_{kj}\delta_{cb}\delta_{\sigma\sigma'} + (kc\sigma|jb\sigma') + f^{\mathrm{xc}}_{kc\sigma jb\sigma'}, \tag{16}$$

$$B^{\mathrm{sol}}_{kc\sigma jb\sigma'} = B^{\mathrm{gas}}_{kc\sigma jb\sigma'}. \tag{17}$$

Solvation effect is included through orbital energies $\{\epsilon^{\mathrm{sol}}_{k\sigma}\}$ obtained by solving Kohn-Sham equation in solution, which is given by Eq. (13). By minimizing $\mathcal{L}$ with respect to C, a Z-vector equation is obtained

$$(\epsilon^{\mathrm{sol}}_{a\sigma} - \epsilon^{\mathrm{sol}}_{i\sigma})Z_{ia\sigma} + H^{+}_{ia\sigma}[Z] = -(Q_{ia\sigma} - Q_{ai\sigma}), \tag{18}$$

and $\mathbf{W}$ is determined by the following equations:

$$W_{ij\sigma} = Q_{ij\sigma} + H^{+}_{ij\sigma}[Z] + 2\epsilon^{\mathrm{sol}}_{i\sigma}\delta_{ij}, \tag{19}$$

$$W_{ia\sigma} = Q_{ai\sigma} + \epsilon^{\mathrm{sol}}_{i\sigma}Z_{ia\sigma}, \tag{20}$$

$$W_{ab\sigma} = Q_{ab\sigma}. \tag{21}$$

In the derivation, we employed the standard notations, which were defined in previous studies.[17,21] The scheme of our method is summarized in Scheme 1. Because $\mathbf{F}^{\mathrm{sol}}$ depends on the density matrix at excited state, we need iterative calculations among Kohn-Sham equation in solution (Eqs. (13) and (14)), TD-DFT equation (Eq. (15)), and Z-vector equation (Eq. (18)).

We can simply obtain the derivative of the excitation energy because variables, $\mathbf{X},\mathbf{Y},\mathbf{C},\mathbf{Z},\mathbf{W}$, and correlation functions in RISM are determined from the stationarity conditions as follows:

$$\begin{aligned}\Delta G^{\xi}_{[\mathrm{E}]} &= \mathcal{L}^{\xi} \\ &= \Delta G^{(\xi)}_{[\mathrm{E}]} + \sum_{ia\sigma} Z_{ia\sigma}F^{\mathrm{sol}(\xi)}_{ia\sigma} - \sum_{pq\sigma,p\le q} W_{pq\sigma}S^{(\xi)}_{pq\sigma}, \\ &= \frac{1}{2}\sum_{i\sigma}(h^{(\xi)}_{ii\sigma} + F^{\mathrm{gas}(\xi)}_{ii\sigma}) + \left\langle X,Y\left|\Lambda^{\mathrm{gas}(\xi)}\right|X,Y\right\rangle \\ &\quad + \sum_{ia\sigma} Z_{ia\sigma}F^{\mathrm{gas}(\xi)}_{ia\sigma} - \sum_{pq\sigma,p\le q} W_{pq\sigma}S^{(\xi)}_{pq\sigma} + \Delta\mu^{(\xi)}_{[E]}.\end{aligned} \tag{22}$$

The superscript (ξ) indicates that MO coefficients are held constant at their zero order values. The derivative of $\Delta\mu^{(\xi)}_{[\kappa]}$ was derived in a previous study.[18]

Although the derived equations appear to be complicated, it is almost the same with the equations obtained in gas phase.[17] By adding the subroutine for the calculation of $\Delta\mu^{(\xi)}_{[\mathrm{E}]}$ and modifying the subroutine of $\mathbf{W}$, we can use the program code prepared for gas phase calculation.[21] For example, we do not have to modify the subroutines implemented in program packages for the calculations of the TD-DFT step (Eqs. (16) and (17)) if we employ solvated orbital energies $\{\epsilon^{\mathrm{sol}}_{k\sigma}\}$ instead of the orbital energies obtained in gas phase. In this study, we employed the standard algorithm[22] implemented in GAMESS program package[23] for the calculations of Eqs. (16) and (17). In the case of 5-cyanoindole, the computational time of the TD-DFT step was 0.7 min both in gas and aqueous phases with CAM-B3LYP/6-311+G(d,p) using 16 cores of a Xeon E5-2630 v3. Because there was no difference between the calculations in gas and aqueous phases, it was confirmed that the additional computational cost of the TD-DFT step in solution is negligible. The simple expression is one of the advantages in our approach. By introducing the relaxation of MOs under the solvation effect determined at the excited state, the complicated terms can be incorporated into orbital energies.

It is better to emphasize the difference between the present study with the previous study by Minezawa.[10] He derived the excited-state free energy on the basis of linear response theory and the correction term is added to consider the relaxation of solvation structure at excited state. In the present study, the relaxation is introduced through a Z-vector equation. Because we derived the gradient on the basis of variational principle, there are no truncated terms in the gradient.

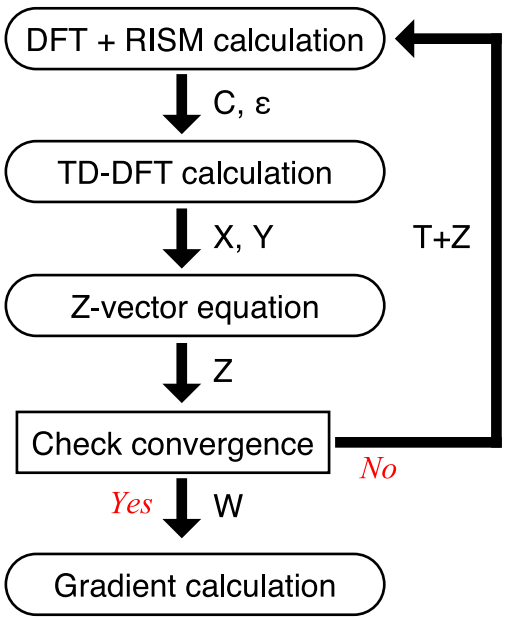

SCHEME 1. Scheme of TD-DFT energy and gradient calculations with RISM-SCF-SEDD.

B. Absorption and emission energies

After the convergence of the iterative calculation in Scheme 1, we can obtain absorption and emission energies, ω^{a} and ω^{f}, as follows:

$$\omega^{\mathrm{a}} = E_{[\mathrm{E}]} - \Delta G_{[\mathrm{G}]}, \tag{23}$$

$$\omega^{\mathrm{f}} = \Delta G_{[\mathrm{E}]} - E_{[\mathrm{G}]}, \tag{24}$$

where $\Delta G_{[\mathrm{G}]}$ is the free energy at ground state. The energy at excited state, $E_{[\mathrm{E}]}$, is defined by

$$E_{[\mathrm{E}]} = \Delta G_{[\mathrm{G}]} + \Omega - \mathbf{V}^{t}_{[\mathrm{G}]}\mathbf{d}_{[Z]} + \mathbf{V}^{t}_{[\mathrm{G}]}(\mathbf{d}_{[\mathrm{E}]} - \mathbf{d}_{[\mathrm{G}]}), \tag{25}$$

where $V_{[G]i}$ is the electrostatic potential on the ith ABS induced by the solvent structure at ground state. In this study, we do not consider the relaxation of solvation structure in absorption. The stabilization at the excited state comes from the relaxation of electron density (the third term) and the interaction change (the fourth term). The energy at ground state can also be defined in the same manner,

$$E_{[G]} = \Delta G_{[E]} - \Omega + \mathbf{V}^t_{[E]}\mathbf{d}_{[Z]} + \mathbf{V}^t_{[E]}(\mathbf{d}_{[G]} - \mathbf{d}_{[E]}). \quad (26)$$

In the emission process, we assume that the relaxation of solvation structure does not occur at ground state.

III. COMPUTATIONAL DETAILS

Solvent data required in RISM-SCF-SEDD calculation were computed with ex-RISM.[24,25] The Lennard-Jones parameters of acetone, indole, and 5-cyanoindole were taken from the OPLS-AA,[26] except for the protic hydrogen attached to N site. We employed the united atom model for AN and MeOH and the SPC-like model for solvent water. The Lennard-Jones parameter σ = 1.0 Å and ϵ = 0.056 kcal/mol was applied to the protic hydrogen sites of solute and solvent molecules. For comparison, we employed the dielectric continuum model, where C-PCM[27] and SMD[28] were employed for electrostatic and non-electrostatic interactions.

The geometries of indole and 5-cyanoindole were optimized in gas phase and each solvent at CAM-B3LYP[29,30]/6-311G(d,p)[31] level. Absorption and emission energies and population analysis were performed with CAM-B3LYP/6-311+G(d,p). About acetone, we performed the calculations with B3LYP/cc-pVDZ, which were employed in previous study.[10]

We performed all calculations with the GAMESS program package, in which our method was implemented.

IV. RESULTS AND DISCUSSION

A. Acetone

In Table I, we summarized some geometric parameters of acetone optimized in aqueous phase. In the optimization calculation at ground state, the difference between Minezawa's and our methods is only the charge fitting process. As shown in previous studies,[12,14] the difference in the charge fitting process is small when the size of basis set is small, which is consistent with the small differences in the optimized structure of acetone at ground state (Table I). Because of the small geometry difference, absorption energies computed with both methods are similar to each other, as shown in Table II.

TABLE I. Selected geometric parameters of acetone in aqueous phase optimized by Minezawa and by the present method. Bond lengths are given in angstroms, angles in degrees, and dipole moments in Debye.

	S_0		$n\pi^*$	
	Minezawa[a]	This work	Minezawa	This work
r(CO)	1.225	1.224	1.309	1.318
r(CC)	1.507	1.508	1.521	1.507
∠CCC	117.2	117.1	117.8	120.1
∠O–CCC	0.0	0.0	36.5	32.3

[a]Reference 10.

TABLE II. Absorption and emission energies computed in aqueous phase (unit: eV).

	ω^a		ω^f	
	Minezawa[a]	This work	Minezawa	This work
Calc.	4.61	4.57	2.96/2.92/3.30[b]	3.14
Exp.	4.68[c], 4.69[d]		3.06[e]	

[a]Reference 10.
[b]ESP-2/ESP-1/ESP-0, see Ref. 10.
[c]Reference 32.
[d]Reference 33.
[e]Reference 34.

On the other hand, the geometry difference at excited state is large compared to the data at ground state. This difference comes from the relaxation of solvent water molecules at excited state. As written in Minezawa's study, the relaxation is partially included in his approach by introducing linear response approach. In our case, the relaxation is completely included under TD-DFT approach by solving the Z-vector equation (Eq. (18)). Minezawa showed that the emission energy was overestimated (3.30 eV) without the solvent relaxation, as shown in Table II. The overestimation was improved by including correction terms (2.96 eV) in his approach. Our computed data (3.14 eV) are between his data.

B. Indole and 5-cyanoindole

Before we discuss the geometries in solution, we focus on the geometries in gas phase. In Table III, the bond lengths optimized in gas phase at ground and excited states (l_g and l_e, respectively) and the differences Δ (=l_e-l_g) for indole and 5-cyanoindole are shown. Atom labels are summarized in Scheme 2. The differences larger than 0.05 are seen in C_2–C_3 and C_6–C_7 of indole and N_1–C_2 C_2–C_3, and C_4–C_5 of 5-cyanoindole.

TABLE III. Optimized bond lengths in gas phase at ground and excited states (l_g and l_e, respectively) and the differences Δ (=$l_e - l_g$). (Unit: angstrom).

	Indole			5-Cyanoindole		
	l_g	l_e	Δ	l_g	l_e	Δ
N_1–C_2	1.38	1.34	−0.03	1.38	1.33	−0.05
N_1–C_8	1.37	1.40	0.03	1.37	1.41	0.04
C_2–C_3	1.36	1.43	0.07	1.36	1.43	0.07
C_3–C_9	1.43	1.41	−0.03	1.43	1.41	−0.02
C_9–C_4	1.40	1.42	0.02	1.39	1.41	0.01
C_4–C_5	1.38	1.42	0.04	1.39	1.44	0.06
C_5–C_6	1.40	1.37	−0.03	1.41	1.40	−0.01
C_6–C_7	1.38	1.45	0.07	1.38	1.41	0.03
C_7–C_8	1.39	1.38	−0.01	1.39	1.40	0.01
C_8–C_9	1.41	1.41	0.00	1.41	1.40	−0.01
C_5–C_c				1.43	1.41	−0.02
C_c–N_c				1.15	1.16	0.01

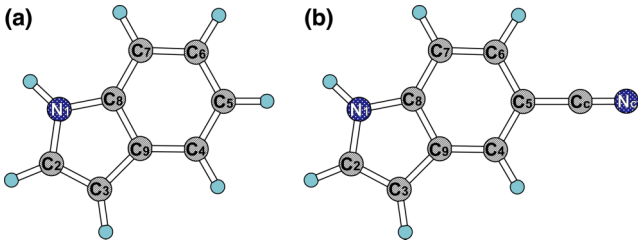

SCHEME 2. Atom labels of (a) indole and (b) 5-cyanoindole.

To discuss the difference in details, we performed the analysis based on resonance structures. In Scheme 3, we showed the resonance structures considered in this study. To answer which resonance structure is dominant in each state, we computed the population of each resonance structures. The approach to determine the population is summarized in the Appendix. In Fig. 1(a), the populations of indole in gas phase at ground and excited states are shown. The most dominant resonance structure at ground state is $R1$, while $R3$ becomes dominant at excited state. The dominant resonance structure changes from $R1$ to $R3$ at the excitation causing the increase of bond length in C_2–C_3 and C_6–C_7, and the decrease of bond length in N_1–C_2, C_3–C_9 and C_5–C_6.

The geometry changes from gas phase to solution phases at excited state are summarized in Table IV. These changes are not so large compared to the changes from ground to excited states (Table III). The largest change in Table IV is seen in the bond C_6–C_7 of 5-cyanoindole. This change can also be explained with resonance structures. In Fig. 1(b), we summarized the resonance structure changes from gas phase to solution phases at excited state. Large changes can be seen in $R2$, $R9$, and $R10$. As the polarity of solvent increases, the populations of $R2$ and $R10$ increase and that of $R9$ decreases. Because the bond indexes of $R2$, $R9$, and $R10$ in the bond

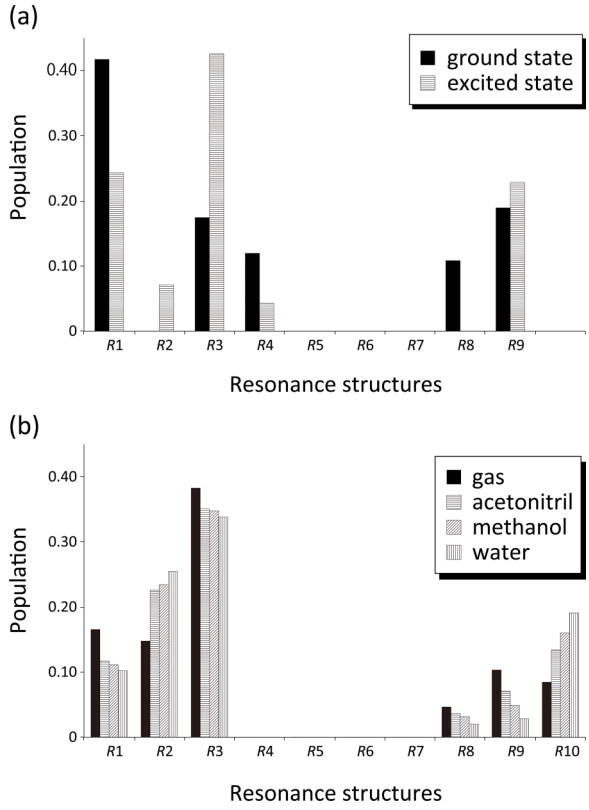

FIG. 1. Populations of resonance structures computed; (a) indole in gas phase at ground and excited states and (b) 5-cyanoindole in solution at excited state.

C_6–C_7 are 2, 1, and 2, respectively, the bond becomes short in polar solvent. This result is reasonable from the fact that $R10$ has a large dipole moment and is stabilized in polar solvent.

The Stokes shifts of indole and 5-cyanoindole were obtained experimentally in various solvents.[35] In this work,

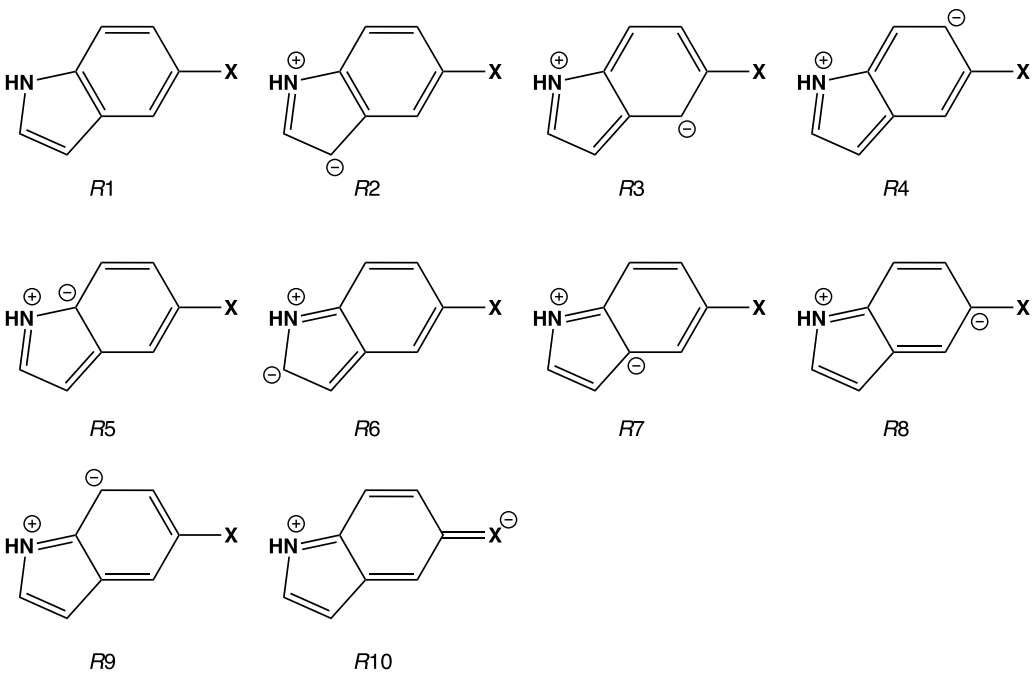

SCHEME 3. Important resonance structures for indole (X = H) and 5-cyanoindole (X = CN). $R10$ is considered only in 5-cyanoindole.

TABLE IV. Bond changes (Δl) from gas phase to solution phase (AN/MeOH/Water) at excited state. (Unit: angstrom).

	Indole Δl	5-Cyanoindole Δl
N_1–C_2	−0.01/−0.02/−0.02	−0.01/−0.01/−0.02
C_2–C_3	0.00/ 0.00/ 0.00	0.00/ 0.00/ 0.00
C_3–C_9	0.01/ 0.01/ 0.02	0.01/ 0.01/ 0.01
C_9–C_4	0.00/ 0.00/−0.01	0.00/ 0.00/ 0.00
C_4–C_5	0.00/ 0.01/ 0.01	0.00/ 0.00/ 0.00
C_5–C_6	0.00/ 0.00/ 0.00	0.01/ 0.01/ 0.02
C_6–C_7	−0.01/−0.01/−0.01	−0.02/−0.02/−0.03
C_7–C_8	0.01/ 0.01/ 0.02	0.00/ 0.00/ 0.01
C_8–C_9	−0.01/−0.01/−0.02	−0.01/−0.01/−0.02
C_5–C_c		−0.01/−0.01/−0.02
C_c–N_c		0.00/ 0.01/ 0.01

we computed the Stokes shifts in AN, MeOH, and water and compared them with the experimental data. First, we compare RISM-SCF-SEDD with RISM-SCF in TD-DFT calculations. In Table V, we summarized the absorption energies to L_a and L_b states (ω_a^a and ω_b^a, respectively), emission energy (ω^f) of 5-cyanoindole. In this comparison, we employed CAM-B3LYP functional and two basis sets, 6-311G(d) and 6-311+G(d,p). When we performed RISM-SCF calculation with the smaller basis set (6-311G(d)), we got converged absorption energies ω^a and they are close to the values computed with RISM-SCF-SEDD. However, when we employed the larger basis set (6-311+G(d,p)), we could not get converged absorption energy in a polar solvent if we use RISM-SCF. Because the atomic charges computed with RISM-SCF diverged in aqueous phase, the instability mainly comes from the problem in the charge fitting process of RISM-SCF, which was discussed in a previous study.[12] In the case of emission energy calculation in aqueous phase, RISM-SCF cannot give emission energy even with the smaller basis set. These results show that SEDD is significantly stable to perform TD-DFT calculations in polar solvent.

To discuss the stability of our method in more detail, we checked basis set dependency and functional dependency in the Stokes shift by employing PBE0 functional[36] and aug-cc-pVDZ[37,38] (Table VI). The results obtained with 6-311+G(d,p) and aug-cc-pVDZ show that the basis set dependency in the Stokes shift is only around 0.02 eV. Compared to basis set dependency, functional dependency is somewhat large. PBE0 underestimates absorption energy and emission energy compared to CAM-B3LYP. Although the difference in the Stokes shift between PBE0 and CAM-B3LYP is around 0.1 eV, both functionals give the same trend that the magnitude of the Stokes shift increases as the polarity increases. Hereafter, we discuss the data computed with CAM-B3LYP/6-311+G(d,p).

In Table VI, we also summarized PCM data for comparison. In the case of absorption energies ω^a, the solvent dependency is small in PCM and our method, which is consistent with experimental data. However, the solvent dependency in the computed emission energies ω^f is different from each other. ω^f computed with our method shifts from 0.85

TABLE V. Absorption energies to L_a and L_b states (ω_a^a and ω_b^a, respectively), emission energy (ω^f) of 5-cyanoindole (unit: eV).

	RISM-SCF						RISM-SCF-SEDD					
	6-311G(d)			6-311+G(d,p)			6-311G(d)			6-311+G(d,p)		
	ω_a^a	ω_b^a	ω^f	ω_a^a	ω_a^b	ω^f	ω_a^a	ω_a^b	ω^f	ω_a^a	ω_a^b	ω^f
AN	4.96	4.80	3.89	4.89	4.73	3.78	4.96	4.81	3.90	4.90	4.73	3.79
MeOH	4.96	4.79	3.70	N/A	N/A	N/A	4.96	4.79	3.75	4.90	4.72	3.70
Water	4.95	4.77	N/A	N/A	N/A	N/A	4.96	4.77	3.51	4.91	4.71	3.48

TABLE VI. Absorption energies (ω_a^a and ω_b^a), emission energy (ω^f), and Stokes shift $\delta\omega$ computed with our method and obtained experimentally (unit: eV).

	This work												PCM							
	CAM-B3LYP								PBE0				CAM-B3LYP							
	6-311+G(d,p)				aug-cc-pVDZ				6-311+G(d,p)				6-311+G(d,p)				exp			
	ω_a^a	ω_b^a	ω^f	$\delta\omega$	ω_a^a	ω_b^a	ω^f	$\delta\omega$	ω_a^a	ω_b^a	ω^f	$\delta\omega$	ω_a^a	ω_b^a	ω^f	$\delta\omega$	ω_a^a	ω_b^a	ω^f	$\delta\omega$
									Indole											
AN	5.08	5.02	4.23	0.85	5.06	4.99	4.21	0.86	5.01	4.82	4.02	0.99	5.05	4.96	4.11	0.94	4.57	4.31	3.88	0.69
MeOH	5.09	5.04	4.18	0.91	5.07	5.00	4.16	0.91	5.02	4.84	3.95	1.06	5.05	4.96	4.11	0.94	4.54	4.32	3.79	0.75
Water	5.12	5.05	4.04	1.07	5.09	5.02	4.03	1.06	5.04	4.85	3.80	1.24	5.05	4.96	4.11	0.94	4.58	4.34	3.57	1.00
									5-cyanoindole											
AN	4.90	4.73	3.79	1.01	4.87	4.71	3.78	1.00	4.75	4.47	3.49	1.06	4.86	4.66	3.92	0.84	4.51		3.48	1.03
MeOH	4.90	4.72	3.70	1.11	4.88	4.70	3.69	1.09	4.76	4.46	3.37	1.18	4.86	4.66	3.92	0.83	4.48		3.42	1.06
Water	4.91	4.71	3.48	1.33	4.88	4.68	3.49	1.30	4.77	4.43	3.14	1.42	4.86	4.66	3.91	0.84	4.51		3.23	1.28

TABLE VII. Dipole moments computed with PCM and our method in each solvent (unit: Debye).

	Indole			5-cyanoindole		
	AN	MeOH	Water	AN	MeOH	Water
PCM	5.73	5.72	5.75	16.10	16.09	16.28
This work	7.07	7.48	8.48	16.14	17.22	19.06

to 1.07 eV (indole) and from 1.01 to 1.33 eV (5-cyanoindole) by changing the solvent. On the other hand, ω^{f} computed with PCM does not show solvent dependency. To explain the difference in ω^{f}, we summarized the dipole moments at excited state in each solvent in Table VII. In the case of our method, the computed dipole moment increases as the solvent becomes polar, while the change of PCM results is small. The underestimation of polarization at excited state in polar solvent by PCM causes the small solvent dependency in ω^{f}.

In Fig. 2, we compared the Stokes shift computed by our method with the experimental one. For comparison, we also added the data computed with PCM in the figure. In the case of indole, the Stokes shift was defined as the difference between emission peak of L_{a} state and absorption energy. On the other hand, it is not easy to assign L_{a} and L_{b} states from experimental data in 5-cyanoindole. To compare our data with experimental data of 5-cyanoindole, we evaluated oscillator strength-weighted absorption energy,[39,40]

$$\omega^{\mathrm{avg}} = \frac{f_{\mathrm{a}}}{f_{\mathrm{a}} + f_{\mathrm{b}}}\omega_{\mathrm{a}}^{\mathrm{a}} + \frac{f_{\mathrm{b}}}{f_{\mathrm{a}} + f_{\mathrm{b}}}\omega_{\mathrm{b}}^{\mathrm{a}}, \tag{27}$$

where f_{a} and f_{b} are the oscillator strengths of L_{a} and L_{b} states, respectively. The Stokes shift of 5-cyanoindole was computed with the following equation:

$$\delta\omega = \omega^{\mathrm{f}} - \omega^{\mathrm{avg}}. \tag{28}$$

The Stokes shift obtained experimentally becomes large as the polarity of the solvent increases. In the case of PCM, the Stokes shift does not show polarity dependence. On the other hand, our method reproduced the Stokes shift change.

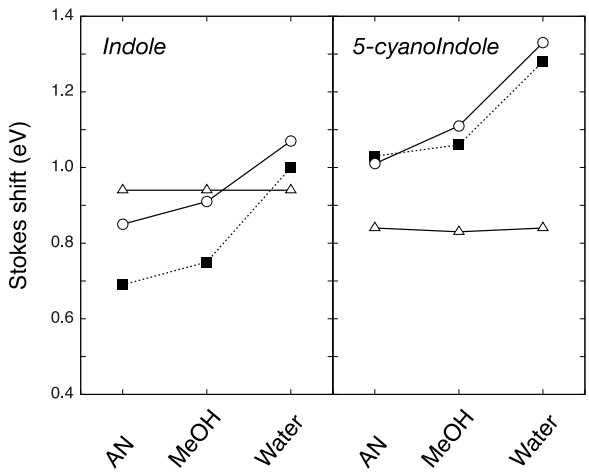

FIG. 2. Stokes shift computed with the present method (open circle) and PCM (open triangle). For comparison, experimental data are also shown (filled square).

TABLE VIII. Emission energies computed with non-relaxed orbitals (unit: eV).

	Indole	5-cyanoindole
AN	4.40	4.07
MeOH	4.42	4.06
Water	4.45	4.04

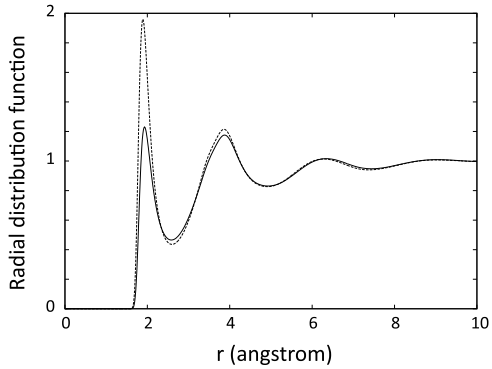

FIG. 3. Radial distribution functions between N_c and water H site of 5-cyanoindole in water at ground state (solid line) at excited state (dotted line).

Why can we reproduce the experimental data about the Stokes shift with RISM-SCF-SEDD? To discuss the origin of the Stokes shift in detail, we computed emission energy ω^{f} with non-relaxed orbitals at excited state (Table VIII). If we do not consider the relaxation of orbitals at excited state, the emission energy does not change so much with respect to the solvent polarity. These results show that the orbital realization at excited state plays a key role and the structure change at excited state is not important in the Stokes shift.

The large Stokes shift in polar solvent can be explained with solvation structure. As shown in Fig. 1 and Scheme 3, the population of the charge separated resonance structure $R10$ increases as the polarity of solvent increases. This is because the large dipole moment of $R10$ is stabilized in polar solvent and the negative charge on N_c site is stabilized by solute-solvent interaction. In Fig. 3, we showed radial distribution functions (RDFs) between N_c and water H site (H_w) of 5-cyanoindole in water at ground and excited states. At the ground state, there is a sharp speak at around $r = 2.0$ Å, which is originated from hydrogen bond between N_c and H_w. The high peak at excited state shows that the solvent effect is enhanced after the excitation. This large difference in the solvent structure is the origin of the large Stokes shift.

V. CONCLUSIONS

We derived the equations for excited state calculations in solution based on RISM-SCF-SEDD and TD-DFT. By employing the Lagrangian approach, the derived equation has a similar formula to those derived in gas phase. This method was applied to the calculation of acetone, indole, and 5-cyanoindole at ground and excited state in solution. The computed geometry is reasonable and the geometry changes were reasonably explained by resonance structures.

The Stokes shift computed with our method reproduced the experimental data.

ACKNOWLEDGMENTS

This work was supported by the Grant-in-Aid for Young Scientists B (Grant No. 24750015) and Scientific Research (C) (Grant No. 15K05385). D.Y. wants to thank Dr. Stephan Irle for providing useful comments.

APPENDIX: LEAST SQUARE FITTING TO DETERMINE THE POPULATIONS OF RESONANCE STRUCTURES

To discuss resonance structures, we defined the expected value of bond order index by

$$\tilde{\mathbf{B}} \equiv \sum_i p_i \mathbf{R}_i, \tag{A1}$$

where $\mathbf{R}_i$ is the bond index defined in ith resonance structure and p_i is the probability to find the ith resonance structure. The probability is determined by minimizing the following target value:

$$\mathcal{L} = |\tilde{\mathbf{B}} - \mathbf{B}|^2 + 2\mu \sum_i \Theta^{(m)}[-p_i], \tag{A2}$$

where $\mathbf{B}$ is the bond order index computed with QM calculation. μ and m are the parameters so that the probability $\{p_i\}$ becomes positive. In this work, we focus of C–N and C–C bonds, and the bond order in $\mathbf{B}$ was computed with Wiberg bond index matrix in the natural atomic orbital (NAO) basis.[41,42] For example, $\mathbf{B}$ and $\mathbf{R}_1$ of indole in gas phase at ground state are (1.148, 1.642, 1.203, 1.314, 1.515, 1.358, 1.504, 1.325, 1.270, 1.134) and (1, 2, 1, 1, 2, 1, 2, 1, 2, 1), respectively.

[1]M. Fernández-Suárez and A. Y. Ting, Nat. Rev. Mol. Cell Biol. **9**, 929 (2008).
[2]H. M. Kim and B. R. Cho, Chem. Rev. **115**, 5014 (2015).
[3]M. E. Casida, *Recent Advances in Density Functional Methods, Part I* (World Scientific, 1995).
[4]T. Helgaker, P. Jørgensen, and J. Olsen, *Molecular Electronic-Structure Theory* (Wiley, 2000).
[5]J. Tomasi, B. Mennucci, and R. Cammi, Chem. Rev. **105**, 2999 (2005).
[6]G. Scalmani, M. J. Frisch, B. Mennucci, J. Tomasi, R. Cammi, and V. Barone, J. Chem. Phys. **124**, 094107 (2006).
[7]S. Ten-no, F. Hirata, and S. Kato, Chem. Phys. Lett. **214**, 391 (1993).
[8]S. Ten-no, F. Hirata, and S. Kato, J. Chem. Phys. **100**, 7443 (1994).
[9]H. Sato, F. Hirata, and S. Kato, J. Chem. Phys. **105**, 1546 (1996).
[10]N. Minezawa, J. Chem. Phys. **138**, 244101 (2013).
[11]T. Wada, H. Nakano, and H. Sato, J. Chem. Theory Comput. **10**, 4535 (2014).
[12]D. Yokogawa, H. Sato, and S. Sakaki, J. Chem. Phys. **126**, 244504 (2007).
[13]K. Iida, D. Yokogawa, H. Sato, and S. Sakaki, Chem. Phys. Lett. **443**, 264 (2007).
[14]D. Yokogawa, Chem. Phys. Lett. **587**, 113 (2013).
[15]A. T. B. Gilbert, N. A. Besley, and P. M. W. Gill, J. Phys. Chem. A **112**, 13164 (2008).
[16]T. Helgaker and P. Jørgensen, Theor. Chim. Acta **75**, 111 (1989).
[17]F. Furche and R. Ahlrichs, J. Chem. Phys. **117**, 7433 (2002).
[18]D. Yokogawa, H. Sato, and S. Sakaki, J. Chem. Phys. **131**, 214504 (2009).
[19]Equation (7) can be rewritten as

$$\Delta G_{[\mathrm{E}]} = \frac{1}{2}\sum_{i\sigma}(h_{ii\sigma} + F^{\mathrm{gas}}_{ii\sigma}) + \langle X, Y|\Lambda^{\mathrm{gas}}|X, Y\rangle + \sum_{ia\sigma} Z_{ia\sigma}F^{\mathrm{gas}}_{ia\sigma} + \Delta\mu_{[\mathrm{E}]}.$$

In the derivation, we employed the following relation:

$$\sum_{ia\sigma} Z_{ia\sigma}F^{\mathrm{sol}}_{ia\sigma} = \sum_{ia\sigma} Z_{ia\sigma}F^{\mathrm{gas}}_{ia\sigma} + V^t_{[\mathrm{E}]}d_{[\mathrm{Z}]} = 0.$$

The physical meanings of the first, second, third, and fourth terms in the first equation are ground state energy, excitation energy, energy change induced by orbital relaxation, and solvation free energy, respectively.
[20]A. D. Becke, J. Chem. Phys. **98**, 1372 (1993).
[21]M. Chiba, T. Tsuneda, and K. Hirao, J. Chem. Phys. **124**, 144106 (2006).
[22]R. E. Stratmann, G. E. Scuseria, and M. J. Frisch, J. Chem. Phys. **109**, 8218 (1998).
[23]M. W. Schmidt, K. K. Baldridge, J. A. Boatz, S. T. Elbert, M. S. Gordon, J. H. Jensen, S. Koseki, N. Matsunaga, K. A. Nguyen, S. Su, T. L. Windus, M. Dupuis, and J. A. Montgomery, J. Comput. Chem. **14**, 1347 (1993).
[24]H. C. Andersen and D. Chandler, J. Chem. Phys. **57**, 1918 (1972).
[25]F. Hirata and P. J. Rossky, Chem. Phys. Lett. **83**, 329 (1981).
[26]W. L. Jorgensen, D. S. Maxwell, and J. Tirado-Rives, J. Am. Chem. Soc. **118**, 11225 (1996).
[27]V. Barone and M. Cossi, J. Phys. Chem. A **102**, 1995 (1998).
[28]A. V. Marenich, C. J. Cramer, and D. G. Truhlar, J. Phys. Chem. B **113**, 6378 (2009).
[29]Y. Tawada, T. Tsuneda, S. Yanagisawa, T. Yanai, and K. Hirao, J. Chem. Phys. **120**, 8425 (2004).
[30]T. Yanai, D. P. Tew, and N. C. Handy, Chem. Phys. Lett. **393**, 51 (2004).
[31]R. Krishnan, J. S. Binkley, R. Seeger, and J. A. Pople, J. Chem. Phys. **72**, 650 (1980).
[32]N. S. Bayliss and E. G. McRae, J. Phys. Chem. **58**, 1006 (1954).
[33]N. S. Bayliss and G. Wills-Johnson, Spectrochim. Acta **24**, 551 (1968).
[34]G. D. Renkes and F. S. Wettack, J. Am. Chem. Soc. **91**, 7514 (1969).
[35]M. Sun and P.-S. Song, Photochem. Photobiol. **25**, 3 (1977).
[36]C. Adamo and V. Barone, J. Chem. Phys. **110**, 6158 (1999).
[37]T. H. Dunning, Jr., J. Chem. Phys. **90**, 1007 (1989).
[38]R. A. Kendall, T. H. Dunning, Jr., and R. J. Harrison, J. Chem. Phys. **96**, 6796 (1992).
[39]When there is a large overlap between (absorption) peaks, the peak position should be affected by the relative intensities of the peaks. To approximate the peak position, the intensity-weighted mean value has been employed (see, for example, Ref. 40). In this study, by assuming that the band widths of the two absorption peaks are the same with each other, we approximated the absorption energy by taking oscillator strength-weighted value.
[40]M. E. Harder, D. A. Malencik, X. Yan, D. Broderick, M. Leid, S. R. Anderson, M. L. Deinzer, and M. I. Schimerlik, Biophys. Chem. **141**, 1 (2009).
[41]K. B. Wiberg, Tetrahedron **24**, 1083 (1968).
[42]A. E. Reed, L. A. Curtiss, and F. Weinhold, Chem. Rev. **88**, 899 (1988).